Science Bulletin 64 (2019) 1601–1607

Contents lists available at ScienceDirect

Science Bulletin

journal homepage: www.elsevier.com/locate/scib

Science Bulletin
www.scibull.com

Article

Anomalous *SmKS* induced by postcritical reflection and refraction at the core-mantle boundary

Liwei Wang [a,b], Fenglin Niu [a,b,*]

[a] State Key Laboratory of Petroleum Resources and Prospecting, and Unconventional Petroleum Research Institute, China University of Petroleum Beijing, Beijing 102249, China
[b] Department of Earth, Environmental and Planetary Sciences, Rice University, Houston, TX 77005, USA

ARTICLE INFO

Article history:
Received 14 July 2019
Received in revised form 24 August 2019
Accepted 26 August 2019
Available online 6 September 2019

Keywords:
SmKS
Hilbert transform
Postcritical phase shift
Outer-core P-wave velocity
Outer core stratification
Ultra-low-velocity-zone

ABSTRACT

Earth's outer core is generally thought to be a well-mixed liquid consisting mostly of iron and a small amount of lighter elements. Recent seismic studies using *SmKS* waves show that the top a few hundred kilometers of the outer core possess a P-wave velocity slightly lower than the PREM model, which cannot be explained by self-compression of a chemically homogeneous outer core. We investigated the *SmKS* waveforms of a deep earthquake occurring beneath South America recorded by a large and dense seismic array in China, and measured the differential arrival times of the *SmKS* pairs. We found significant waveform distortion of the *SmKS* caused by postcritical refraction and reflection at the core-mantle boundary. This waveform distortion can introduce significant bias to the measured differential times, leading to incorrect estimate of P-wave velocity of the outer core. Whether stable stratification is occurring in outer core or not requires further seismic investigations.

1. Introduction

The Earth's outer core is known to be composed primarily of liquid iron with a small amount of light elements, which are well mixed due to its vigorous convection. Hence, it is generally considered to be compositionally homogeneous [1]. The exact concentration of light elements and its depth variation are, however, still not well constrained [2–4]. A recent study on the equation of state and thermodynamic properties of liquid iron using *ab initio* molecular dynamics simulations [5] suggested that the calculated pressure gradient of the P-wave velocity inside the outer core is significantly different from that of the PREM (preliminary reference Earth model) [6], suggesting that concentration of light elements might vary with depth. Thus, accurate knowledge of the 1-D P-wave velocity structure of Earth's outer core is of great importance for understanding its composition, dynamics and evolution.

The series core-reflection phases, *SKS*, *SKKS* (*S2KS*), *S3KS* (hereafter referred as to *SmKS*, $m = 1, 2, 3\cdots$), are widely used in studying the P-wave velocity of the outermost outer core [7–9]. The *SmKS* waves travel across the mantle as shear waves and the outer core as compressional waves (Fig. 1a). They are reflected $(m-1)$ times from the lower side of the core-mantle boundary (CMB) and can be observed at a wide range of epicentral distances, i.e., ~85°–180° (Fig. 1a). Differential traveltimes between *SmKS* pairs, such as *S3KS* and *S2KS*, *S4KS* and *S3KS*, are usually employed in constraining the P-wave velocity structure in the top part of the outer core as these pairs have very similar propagating paths in the mantle. Since there is a $\pi/2$ phase shift between two consecutive *SmKS* arrivals due to the internal caustic surface for underside reflection [10], measuring the differential times between the two arrivals using waveform cross-correlation requires an operation of Hilbert transform of the first arrival before taking the regular cross-correlation of the two phases.

Many seismic studies found that the *SmKS* differential traveltimes are slightly larger that the PREM predictions, which was interpreted to mean that the top few hundred kilometers of the outer core possess a P-wave velocity slightly lower than that of the PREM [11–17]. Based on the slower-than-PREM P-wave velocity profile in the topmost ~ 300 km of the outer core, Helffrich and Kaneshima [15] argued that this outermost layer might be compositionally distinct from the rest of the outer core, with a higher concentration of light elements that leads to the observed low P-wave velocity. On the other hand, Alexandrakis and Eaton [18] employed an empirical transfer function (ETF) technique and measured the differential traveltimes from the stacked data and found that differential traveltime residuals with respect to the PREM are insignificant. Therefore, the PREM provides the best fit to the observed traveltime residuals. Tanaka [14] found that S-wave velocity structures in the lowermost mantle could also affect the

* Corresponding author.
E-mail address: niu@rice.edu (F. Niu).

https://doi.org/10.1016/j.scib.2019.09.004
2095-9273/

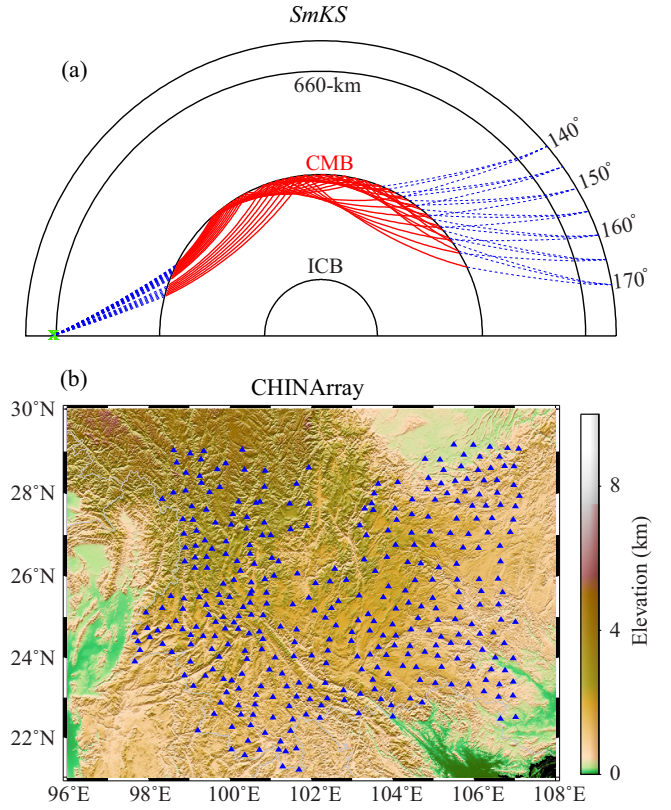

Fig. 1. *SmKS* raypaths and the phase-I CHINArray. (a) Ray paths of the *SmKS* waves (*S2KS*, *S3KS* and *S4KS*) at epicentral distances of 140°–170°. *SmKS* waves travel across the mantle as shear waves (blue dashed lines) and the outer core as compressional waves (red solid lines). Their ray paths in the mantle are very close to each other; therefore their differential traveltimes have been used to investigate the P-wave velocity structure in the outermost outer core. (b) Geographic locations of the broadband seismic stations deployed in the first phase of the CHINArray project. Seismometers were deployed for a period of 2 years with a spacing of ~30 km.

SmKS waveforms, leading to anomalies in differential traveltime residuals.

We observed clear *S2KS*, *S3KS*, and *S4KS* with high signal-to-noise ratio (SNR) from individual seismograms of a deep earthquake occurring in South America recorded by a large and dense seismic array in China. We noticed that waveforms of *S2KS* and *S3KS* arrivals from the major arc direction are almost identical, instead of showing a $\pi/2$ phase shift. Numerical modeling suggested that the lack of the anticipated Hilbert transform is likely caused by a postcritical-reflection induced phase shift of the *S2KS* arrivals that are reflected at the CMB beneath the Pacific large low velocity province (LLVP). Measuring *S3KS*–*S2KS* differential times using the regular cross-correlation method after performing the Hilbert transform can introduce a ~0.6 s positive residual, therefore, it is important to take into account anomalous structures in the lowermost mantle while interpreting the *SmKS* differential traveltime data for outer core P-wave velocity structure.

2. *SmKS* recorded by the CHINArray

The large and dense broadband array we used in this study is the first phase deployment of the CHINArray project that covered the southeast margin of the Tibetan Plateau (Fig. 1b). The temporal array consisted of ~350 stations, and was deployed between 2011 and 2013 with a station spacing of ~30–40 km. Each seismograph is equipped with a Guralp CMG-3ESP seismometer and a Reftek-130 data logger. Owing to a favorable mechanism, the *M*w 6.7 deep earthquake that occurred on May 28 of 2012 (PDE: 05/28/2012 05:07:23.45, 28.043°S, 63.094°E, 586.9 km deep, *M*w 6.7) generated strong *SmKS* waves that are clearly recorded by the CHINArray. In particular, *S2KS* and *S3KS* recorded in the epicentral distance range of ~166°–172° from the major arc direction (hereafter referred to as *S2KS2* and *S3KS2*, respectively) possess the highest SNR on the radial component (Fig. 2a), which allows for precise measurements of the *S3KS2*-*S2KS2* differential times. *S2KS* and *S3KS* from the minor arc direction were also observed, but were not used because of their generally low amplitudes. The underside reflection points of *S2KS2* shown in Fig. 2b are located within the Pacific LLVP [19,20], where Cottaar and Romanowicz [21] found an ultra-low-velocity-zone (ULVZ) at the base of the mantle.

The seismograms shown in Fig. 2a are aligned by the arrival times of *S2KS2*, which are set to zero. The red and green solid squares indicate the arrival times of *S3KS2* and *S4KS2* calculated by the PREM. We noticed that the *S2KS2* and *S3KS2* waveforms are similar to each other, which is unpredicted by 1D reference models such as the PREM. To show this, we first aligned the *S2KS2* and *S3KS2* waveforms along their peaks and then stacked them separately. The stacked *S2KS2* and *S3KS2* are shown in the top and bottom panels of Fig. 2c, respectively. For comparison, we also showed the Hilbert-transformed *S2KS2* in the middle. It is clear that the *S3KS2* waveform shown in the bottom of Fig. 2c matches the *S2KS2* better than its Hilbert transform, suggesting that one or both of the two phases experienced some distortion along their propagating paths.

3. Analyses and results

3.1. Postcritical phase shifts

The ray paths of *SmKS* (from either the minor or major arcs) shown in Fig. 1a indicate that the entry S-to-P refraction, the underside P-to-P reflection, and the exiting P-to-S refraction at the CMB all could potentially introduce phase shifts if the incident angles are larger than their corresponding critical reflection/refraction angles, which are 31.99°, 36.06°, and 36.06°, respectively, based on the PREM. Indeed, 1-D ray tracing with the PREM suggests that *S2KS* and *S3KS* waves recorded at epicentral distances of 120°–170° traverse across the CMB in postcritical reflection/refraction angles. Fig. 3a shows the phase shifts of *S2KS* and *S3KS* during the S-to-P refraction and P-to-P reflection at the CMB. The phase shifts of the P-to-S refraction at the CMB exit points are expected to be similar to those of the S-to-P transmission at the CMB entrance points. The calculated phase shifts are highly nonlinear with respect to the incident angle and epicentral distance. Overall, the phase delays are less than 10° except for the postcritical reflection of *S2KS* at epicentral distances greater than 160°. We further computed the total phase shifts of the two phases due to refraction and reflection, as well as the *S3KS*–*S2KS* differential phase shifts, which are shown in purple dash-dotted line in Fig. 3a. The differential phase shift of the PREM varies between ~−20° and ~10°, much smaller than the expected 90° phase shift caused by the internal caustics.

As the critical refraction angles of S-to-P and P-to-S and the critical reflection angle of P-to-P are all highly sensitive to the velocity structure at the base of the mantle, we generated a 1-D ULVZ model that has a 150-km thick low-velocity layer at the base of the mantle. S-wave velocity drops from the PREM by 0% at the top of the layer and linearly increases to 10% at the bottom of the layer. We further reduced the S-wave velocity by another 20% within the bottom 10 km of the layer. The S-wave velocity profile of the ULVZ model is shown in Fig. 3b, together with the PREM

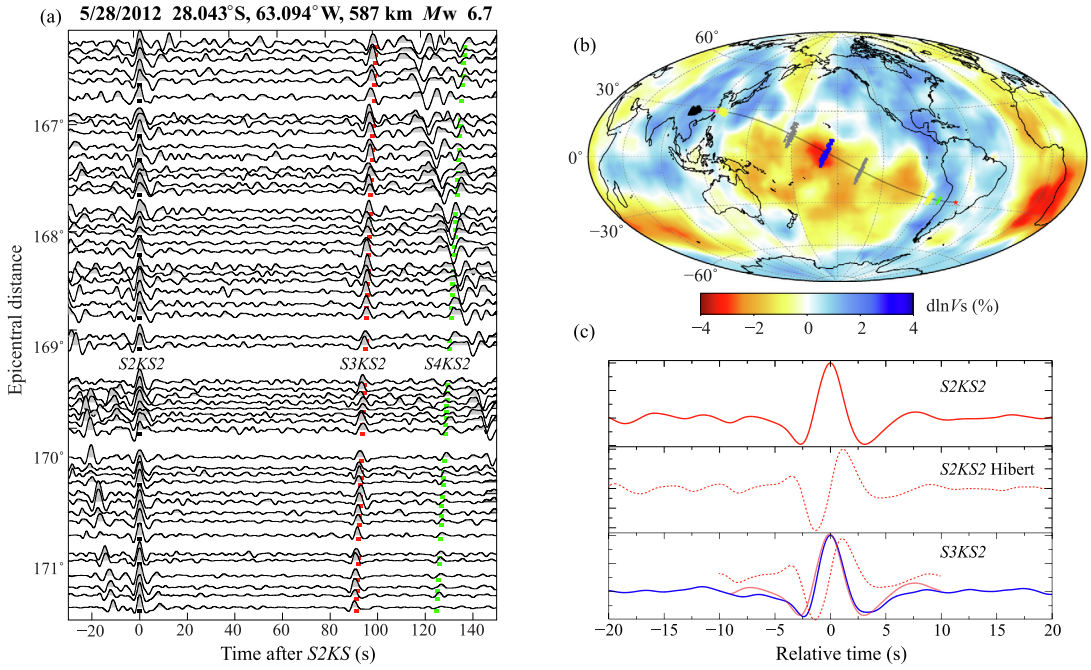

Fig. 2. *SmKS* waves recorded by the CHINArray. (a) Examples of the *SmKS* recorded on the radial component of the CHINArray. Seismograms are aligned at the peak of *S2KS2*. PREM predictions of the *S3KS2* and *S4KS2* arrival times are indicated by red and green dots, respectively. (b) Geographic map showing the piercing points of *S2KS2* and *S3KS2* ray paths at the CMB from the 05/28/2012 *M*w 6.7 South American deep earthquake (red star) to the CHINArray stations (black triangles). The green, blue and pink points represent the CMB entrance, reflection and exit points of the *S2KS2* waves, respectively. The yellow circles and grey triangles represent, respectively, the CMB entrance/exit and reflection points of the *S3KS2* waves. Color contours show the shear-wave velocity anomalies of the D″ layer (Grand, 2002). (c) A comparison of stacked *S2KS* (red solid line), Hilbert transformed *S2KS2* (red dash line) and *S3KS2* (blue solid line). Note the *S3KS2* phase shows a similar waveform of the *S2KS2*, instead of the expected Hilbert transform of *S2KS2*.

model for comparison. The P-wave and density of the ULVZ model was kept same as those of the PREM.

The computed postcritical phase shifts of the *S2KS* and *S3KS* within the ULVZ model are shown in Fig. 3c, and are much larger than those of the PREM. The underside P-to-P reflection coefficients of the *S2KS* can generate a phase shift of greater than 30° when the epicentral distance reaches beyond 150° (black dotted line in Fig. 3c). The calculated *S3KS*–*S2KS* differential phase shift of the ULVZ model is plotted in purple dash-dotted line in Fig. 3c, which changes from −10° at the epicentral distance of 120° to −80° at the distance of 170°. These large phase shifts can generate significant changes in the *SmKS* waveforms and their differential traveltimes.

3.2. 1-D waveform modeling of SmKS

In order to quantify the postcritical phase shifts of S-to-P and P-to-S refractions and P-to-P reflections and their induced anomalies in *SmKS* waveforms and differential traveltimes, we employed the 2-D spectral-element method, AxiSEM [22,23], to compute synthetic *SmKS* waveforms. The AxiSEM code solves 3-D wave propagation in an spherically symmetric medium by collapsing the 3-D sphere into a 2-D disk, which can significantly raise the computational efficiency [22,23]. We computed the 1-D synthetics with the AxiSEM code for both the PREM and ULVZ models. For each model, a point source was placed at 0° longitude on the equator with a depth of 550 km, while receivers were deployed along the equator in the longitudinal range of 120°–180° with an interval of 0.1°. The AxiSEM synthetics appeared to be very noisy at epicentral distances greater than 170°, and thus were not used in our investigation. A dip slip fault ($\delta = \pi/2$, $\lambda = -\pi/2$) with a strike of 0° was employed as the source mechanism. Fig. 4a and b shows part of the synthetic *SmKS* in the epicentral distances of 150°–160° of the PREM and ULVZ models, respectively. The data shown here were band-pass filtered with a two-pole Butterworth filter in the period band of 2–50 s. As our purpose is to investigate how postcritical phase shifts affect the waveforms of the *S2KS* and *S3KS* and their differential traveltimes, we used the arrivals from the minor arc, which has much better SNR than those from the major arc in the AxiSEM synthetics. The major-arc *SmKS* arrivals appeared to be very weak in the AxiSEM synthetics, and therefore might not have been correctly computed.

In Fig. 4c, we further show a comparison of waveform similarity between the PREM synthetics; the waveforms shown from the top to bottom are the *S2KS*, the polarity-reversed *S3KS* Hilbert transform, the *S2KS* Hilbert transform, and the *S3KS*, respectively. It is clear that the *S2KS* and *S3KS* waveforms are highly similar to the polarity-reversed and normal Hilbert transforms of the *S3KS* and *S2KS*, respectively, which are highlighted in the top and bottom of the panel. On the other hand, a similar comparison of the ULVZ synthetics (Fig. 4d) shows that the waveforms of the *S2KS* and *S3KS* are similar to each other, rather than to the Hilbert transforms of the other phases, suggesting that the postcritical refraction and reflection induced phase shifts to *SmKS* are significant enough to result in a π/2. This is consistent with the total phase shift estimated from the postcritical reflection and refraction described in the previous section.

3.3. Influence on SmKS differential traveltimes

In order to quantify the influence of the postcritical phase shifts on *S3KS*–*S2KS* differential traveltimes, we employed the regular cross-correlation based method to estimate the differential times (hereafter referred as to $\Delta T_{(S3KS-S2KS)C}$). We also ray traced the two waves propagating through the PREM and ULVZ models and computed the theoretical *S3KS*–*S2KS* differential time (hereafter

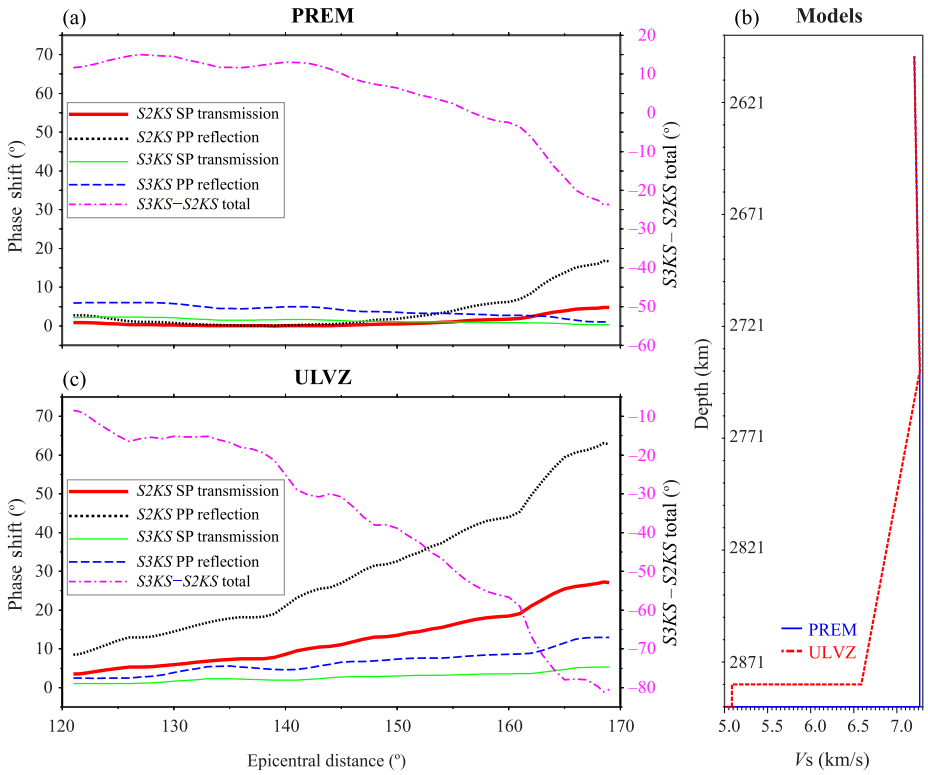

Fig. 3. Postcritical phase shifts of *SmKS* calculated from the PREM and ULVZ models. (a) Postcritical phase shifts of the minor-arc *S2KS* and *S3KS* waves traveling in the PREM model are shown as a function of epicentral distance. The red solid line and black dotted line represent, respectively, the phase shifts of the S-to-P refraction and the underside P-to-P reflection of the *S2KS* waves at the CMB, while the green solid line and blue dashed lines indicate those of the *S3KS* waves. The purple dash-dotted line is the *S3KS*−*S2KS* differential phase shifts. The left and right vertical axes show the scales of the individual and differential phase shifts, respectively. (b) A comparison of the S-wave velocity in the bottom 290 km of the mantle between the PREM (blue solid line) and the ULVZ (red dotted line). The ULVZ model has a 150-km thick D″ layer with a reduced S-wave velocity that drops linearly from 0% to 10%, and a 10-km ultra-low-velocity zone at the bottom of the mantle that has an S-wave velocity 30% lower than that of the PREM. (c) Similar to (a) except for *SmKS* propagating through the ULVZ model.

referred as to $\Delta T_{(S3KS-S2KS)R}$). We further defined the differential traveltime residuals with respect to the PREM as

$$\delta t_{(S3KS-S2KS)\mathrm{PREM}} = \Delta T_{(S3KS-S2KS)C} - \Delta T_{(S3KS-S2KS)\mathrm{RPREM}}. \quad (1)$$

Fig. 5a shows *S3KS-S2KS* differential traveltime residuals measured from the synthetics of the PREM and ULVZ models. More specifically, we first applied the Hilbert transform to all the synthetic *S2KS* waveform data of the two models, and then used the transformed waveforms as templates to correlate them with the *S3KS* waveforms. The differential times, $\Delta T_{(S3KS-S2KS)C}$, were obtained when the cross-correlation coefficient reaches the maximum. We found that the ray tracing differential times of the ULVZ model ($\Delta T_{(S3KS-S2KS)\mathrm{RULVZ}}$) are about ~0.6 s larger than those of the PREM ($\Delta T_{(3SKS-S2KS)\mathrm{RPREM}}$). The blue dotted line plotted in Fig. 5a shows the difference of the two models as a function epicentral distance. The differential traveltime residuals from the PREM synthetics (black open circles in Fig. 5a) exhibit a systematic positive value of ~0.05 s, decay to 0.00 at an epicentral distance of ~155° and further decrease almost linearly to −0.20 s at the distance of 170°. This trend correlates well with the variations of the *S3KS*−*S2KS* differential phase shift shown in Fig. 3a.

Meanwhile, the differential traveltime residual (red solid squares in Fig. 5a) measured with the ULVZ synthetics reaches ~0.60 s and monotonically decreases with epicentral distance and reduces to ~0.20 s at the epicentral distance of 170°. Since the measured differential traveltime residuals (red solid squares in Fig. 5a) here are the combined effects of the ULVZ velocity structure (blue dotted line in Fig. 5a) and the postcritical phase shifts, therefore the phase-shift effect (difference between the blue dotted line and the red solid squares) increases from ~0.0 s at 120° to ~ 0.5 s at 170°, which is also consistent with the large *S3KS*−*S2KS* differential phase shifts of the ULVZ model shown in Fig. 3c.

We further designed a filter that corrects waveform distortions induced by the postcritical reflection and refraction, and applied it to the synthetic *SmKS* waveform data. To do so, we first took the Fourier transform of *SmKS* data and then applied a phase shift to the complex spectrum by multiplying it with $\exp\{-i\phi\}$, where ϕ is the postcritical phase shift calculated in Section 3.1. Finally, we applied an inverse Fourier transform to the corrected Fourier spectrum, and obtained the corrected *SmKS* waveform data. We then employed the same steps in measuring *S3KS*−*S2KS* differential times from the corrected *SmKS* waveform data and computed the differential traveltime residuals of the PREM and ULVZ models, which are shown as black open circles and red solid squares in Fig. 5b, respectively. The *S3KS*−*S2KS* differential time residuals computed from the PREM synthetics are close to zero (grey solid line), while those measured from the corrected *SmKS* synthetics of the ULVZ model are very close to the blue dotted line. Both the grey solid zero line and the blue dotted line are the ray theory predictions of the differential traveltime residuals of the two models.

4. Discussion

Our analyses clearly showed that the differential *SmKS* traveltimes can be signficantly affected by anomalous velocity structures in the lowermost mantle. The influence comes from two aspects: (1) traveltime anomalies induced by 3-D S-wave velocity hetero-

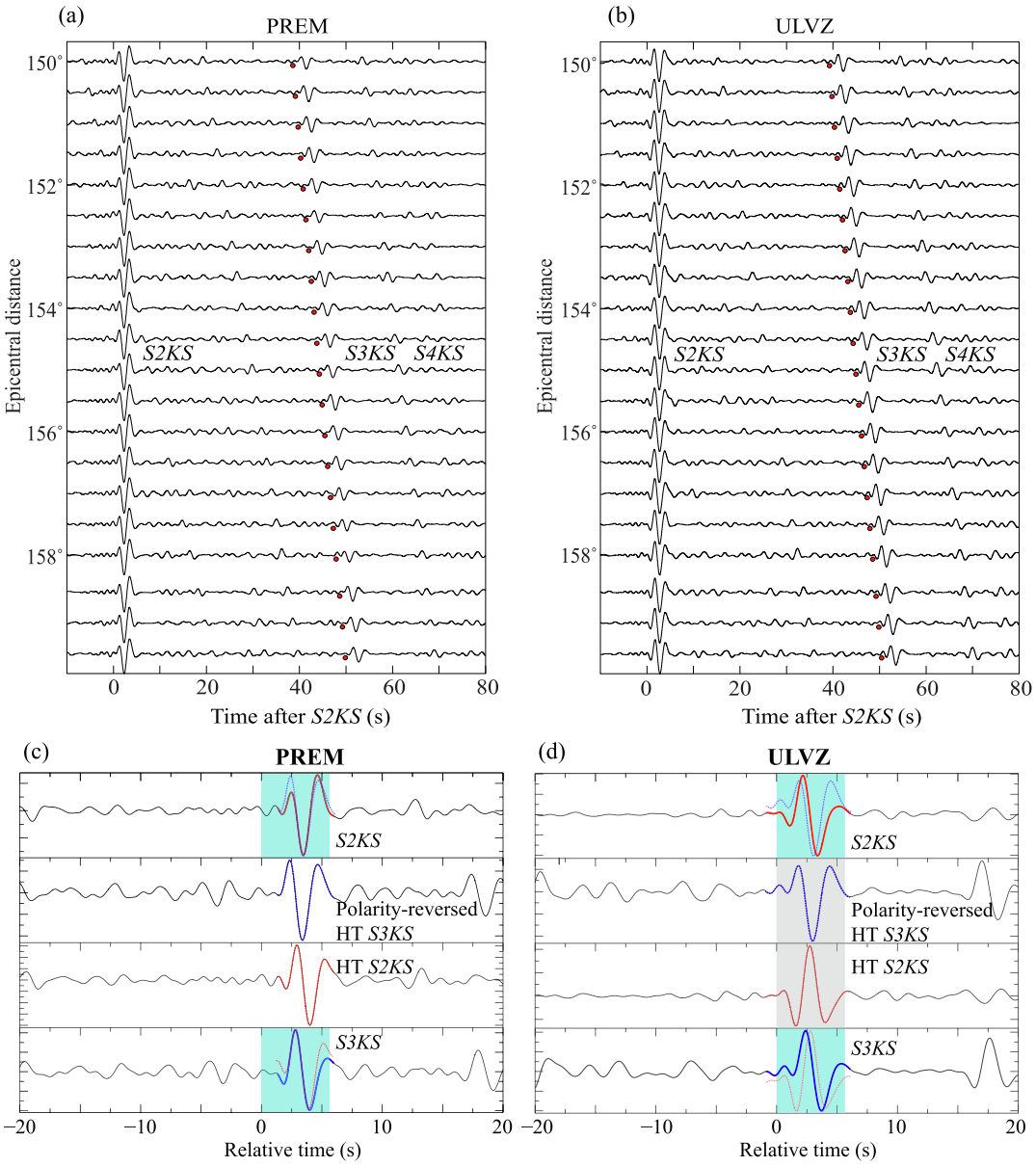

Fig. 4. (Color online) Synthetic *SmKS* waves of the PREM and ULVZ models. Radial component synthetic seismograms calculated from the PREM and ULVZ models are shown in the left (a) and right (b) panels, respectively. PREM and ULVZ predictions of the *S3KS* arrival times are indicated by red dots. (c), (d) Enlarged waveforms of the *S2KS* and *S3KS* are shown together with their Hilbert transforms. Note that the PREM S3KS (c) matches with the Hilbert-transformed *S2KS*, while the ULVZ *S3KS* fits with the *S2KS* directly.

geneties in the lowermost mantle; (2) phase shifts due to postcritical refraction and reflection at the CMB, which are related to both the S- and P-wave velocities right above the CMB. The latter is highly nonlinear, and is related to velocity contrasts at the CMB near the entrance, reflection and exit points. Therefore it is very challenging to constrain lowermost mantle velocity structures by using anomalous *SmKS* waveforms and differential times alone.

The *S3KS2*−*S2KS2* differential traveltime residuals estimated from the records of the 5/28/2012 *M*w 6.7 events are between −1.57 and −0.18 s with an average of −0.76 s. The measurements are obtained by cross correlating the two arrivals without performing a Hilbert transform of the *S2KS2* waves. The negative residuals are inconsistent with outer core models that have a low velocity layer in the top. We noticed that both the entrance and exit points of the *S2KS2* (green and purple points in Fig. 2b) and *S3KS2* (yellow circles) are located inside D″ regions charaterized by a high S-wave velocity [19]. Since the ULVZ model, which has very low S-wave velocity at the base of the mantle, can introduce positive differential traveltime residuals only in the order of ∼0.6 s, it would be difficult to attribute the observed −0.76 s negative residuals to 3-D S-wave high-velocity anomalies in the lowermost mantle. It is plausible that some portion of the observed residuals is caused by postcritical phase shifts of the two waves.

The incident angles of the *S2KS2* recorded at epicentral distances of ∼162.3° are, however, less than the corresponding critical angles of the down going S wave above the CMB and the up going P wave below the CMB in both the PREM and ULVZ models. On the other hand, the observed *S3KS2* waves are expected to undergo postcritical refractions and reflections. However, the postcritical phase shifts of the *S3KS2* would cause to delay its arrival time, leading to positive *S3KS2*−*S2KS2* differential traveltime residuals. In order to lower the critical angles down to the incident angles of the observed *S2KS2* waves, the P-wave velocity at the base of the mantle must be ∼6% higher than that of the PREM. To our

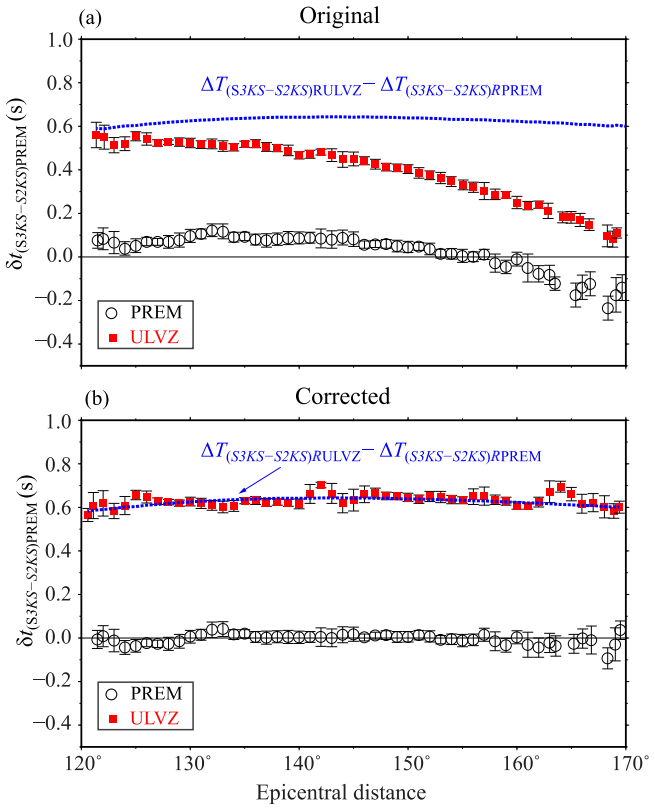

Fig. 5. (Color online) Differential *SmKS* traveltime residuals. (a) *S3KS–S2KS* differential traveltime residuals of the PREM and ULVZ synthetics at the epicentral distance range of 120°–170° are shown in black open circles and red solid squares, respectively. The differential traveltimes are measured by cross correlating *S3KS* with Hilbert-transformed *S2KS*. The thin black solid zero line and the thick blue dotted line represent the differential traveltime residuals calculated by ray theory. Note the large discrepancy between the red solid squares and the blue dotted line at large epicentral distances. (b) *S3KS–S2KS* differential traveltime residuals measured from the corrected PREM and ULVZ synthetics (see main text for the details on the correction of postcritical phase shifts). All the symbols are similar to (a). Note the good agreement between the measured differential traveltime residuals (black open circles and red solid squares) and the ray theory predictions (thin black solid line and thick blue dotted line).

knowledge, no such high P-wave velocity anomalies have been observed at the base of the mantle. One possible senario is that the CMB beneath the central Pacific (blue solid squares in Fig. 2b) is not flat. Our calculation suggested that if the CMB is tilted by ~2°, then the observed *S2KS2* can experience large postcritical phase shift during underside P-to-P reflection, which can significantly reduce the *S3KS2–S2KS2* differential traveltimes. However, any anomalous structures at the entry and exit points of *S2KS2* can also cause postcritical phase shifts during the S-to-P and P-to-S refractions, and future 3-D modeling and inversion [24] is required to use the waveforms of *S2KS2* and *S3KS2* to constrain CMB structures.

5. Conclusions

We observed clear *SmKS* arrivals on seismograms of the CHINArray from a deep earthquake occurring in South America. There is a lack of π/2 phase shift in the waveforms of the major-arc *S2KS2* and *S3KS2* arrivals. Our traveltime analysis and waveform modeling suggested that postcritical S-to-P and P-to-S refractions and underside P-to-P reflection at the CMB can introduce large phase shifts to the *SmKS* waveforms. When a ULVZ is present in the base of the mantle, it can cause a differential phase shift close to π/2 between the *S2KS* and *S3KS* at some epicentral distances, which means that the two phases should possess nearly identical waveforms. We also found that *SmKS* differential traveltimes can be significantly affected by 3-D S-wave heterogeneities in the lowermost mantle, as well as postcritical phase shifts that are sensitive to P- and S-wave velocity contrast across the CMB. Therefore, we must take special cautions when we use *SmKS* differential traveltime residuals to constrain outer core P-wave velocity structure.

Conflict of interest

The authors declare that they have no conflict of interest.

Acknowledgments

This work was jointly supported by the National Key Research and Development Program of China (2017YFC1500303) and the National Natural Science Foundation of China (41630209). We thank the Data Management Center of China Seismic Array at the Institute of Geophysics, China Earthquake Administration (ChinArray DMC, https://doi.org/10.12001/ChinArray.Data) for providing the waveform data. We thank the Associate Editor and the anonymous reviewers for their constructive comments and suggestions, which significantly improved the quality of this paper.

Author contributions

Liwei Wang conducted the analysis and interpretation; Fenglin Niu contributed to the interpretation and took the lead on writing the manuscript.

References

[1] Stevenson DJ. Limits on lateral density and velocity variations in the Earth's outer core. Geophys J Roy Astron Soc 1987;88:311–9.
[2] Poirier JP. Light elements in the Earth's outer core: a critical review. Phys Earth Planet Int 1994;85:319–37.
[3] Morard G, Siebert J, Andrault D, et al. The Earth's core composition from high-pressure density measurements of liquid iron alloys. Earth Planet Sci Lett 2013;373:169–78.
[4] Zhang Y, Sekine T, He H, et al. Experimental constraints on light elements in the Earth's outer core. Sci Rep 2016;6:22473.
[5] Ichikawa H, Tsuchiya T, Tang Y. The P-V-T equation of state and thermodynamic properties of liquid iron. J Geophys Res 2014;119:240–52.
[6] Dziewonski AM, Anderson DL. Preliminary reference Earth model. Phys Earth Planet Int 1981;25:297–356.
[7] Souriau A, Poupinet G. A study of the outermost liquid core using differential travel times of the *SKS*, *SKKS* and *S3KS* phases. Phys Earth Planet Int 1991;68:183–99.
[8] Garnero EJ, Helmberger DV, Grand SP. Constraining outermost core velocity with *SmKS* waves. Geophys Res Lett 1993;20:2463–6.
[9] Tanaka S, Hamaguchi H. Degree one heterogeneity at the top of the Earth's core, revealed by *SmKS* travel times. In: Le Mouel JL, Smylie DE, Herring T, editors. Dynamics of Earth's deep interior and Earth rotation, geophysical monograph series. Washington, DC: American Geophysical Union; 1993. p. 127–34.
[10] Choy GL. Theoretical seismograms of core phases calculated by frequency-dependent full wave theory, and their interpretation. Geophys J Roy Astron Soc 1977;51:275–312.
[11] Lay T, Young CJ. The stably stratified outermost outer core revisited. Geophys Res Lett 1990;17:2001–4.
[12] Souriau A, Teste A, Chevrot S. Is there any structure inside the liquid outer core? Geophys Res Lett 2003;30:1567.
[13] Eaton DW, Kendall JM. Improving seismic resolution of outer- most core structure by multichannel analysis and deconvolution of broad-band *SmKS* phases. Phys Earth Planet Int 2006;155:104–19.
[14] Tanaka S. Possibility of a low P-wave velocity layer in the outermost core from global *SmKS* waveforms. Earth Planet Sci Lett 2007;259:486–99.
[15] Helffrich G, Kaneshima S. Outer-core compositional stratification from observed core wave speed profiles. Nature 2010;468:807–10.
[16] Kaneshima S, Helffrich G. *Vp* structure of the outermost core derived from analyzing large-scale array data of *SmKS* waves. Geophys J Int 2012;93:1537–55.
[17] Tang V, Zhao L, Hung SH. Seismological evidence for a non-monotonic velocity gradient in the topmost outer core. Sci Rep 2015;5:8613.

[18] Alexandrakis C, Eaton DW. Precise seismic-wave velocity atop Earth's core: no evidence for outer-core stratification. Phys Earth Planet Int 2010;180:59–65.
[19] Grand SP. Mantle shear-wave tomography and the fate of subducted slab. Philos Trans Roy Soc London A 2002;360:2475–91.
[20] Niu Y, Shi X, Li T, et al. Testing the mantle plume hypothesis: an IODP effort to drill into the Kamchatka-Okhotsk Sea basement. Sci Bull 2017;62:1464–72.
[21] Cottaar S, Romanowicz B. An unusually large ULVZ at the base of the mantle near Hawaii. Earth Planet Sci Lett 2012;355–356:213–22.
[22] Nissen-Meyer T, Fournier A, Dahlen FA. A 2-D spectral-element method for computing spherical-earth seismograms—I moment-tensor source. Geophys J Int 2007;168:1067–93.
[23] Nissen-Meyer T, Fournier A, Dahlen FA. A 2-D spectral-element method for computing spherical-earth seismograms—II. Waves in solid-fluid media. Geophys J Int 2008;174:873–88.
[24] Wang J, Yang DH, Jing H, et al. Full waveform inversion based on the ensemble Kalman filter method using uniform sampling without replacement. Sci Bull 2019;64:321–30.

Liwei Wang is a Ph.D. degree candidate at China University of Petroleum-Beijing. Her research interests include the structure of core-mantle boundary, mantle transition zone and the origin of Datong volcano. She holds a bachelor degree of geo-information science and technology from the Central South University.

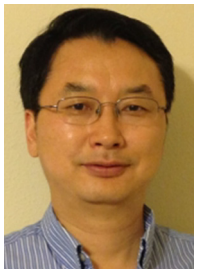

Fenglin Niu is a professor at Rice University and China University of Petroleum-Beijing with a primary focus on determining the seismic structure of Earth's deep interior, especially the fine seismic structures of the boundary layers.